Arc Distribution During the Vacuum Arc Remelting of Ti-6Al-4V

C. RIGEL WOODSIDE, PAUL E. KING, and CHRIS NORDLUND

Currently, the temporal distribution of electric arcs across the ingot during vacuum arc remelting (VAR) is not a known or monitored process parameter. Previous studies indicate that the distribution of arcs can be neither diffuse nor axisymmetric about the center of the furnace. Correct accounting for the heat flux, electric current flux, and mass flux into the ingot is critical to achieving realistic solidification models of the VAR process. The National Energy Technology Laboratory has developed an arc position measurement system capable of locating arcs and determining the arc distribution within an industrial VAR furnace. The system is based on noninvasive magnetic field measurements and a VAR specific form of the Biot–Savart law. The system was installed on a coaxial industrial VAR furnace at ATI Albany Operations in Albany, OR. This article reports on the different arc distributions observed during production of Ti-6Al-4V. It is shown that several characteristic arc distribution modes can develop. This behavior is not apparent in the existing signals used to control the furnace, indicating the measurement system is providing new information. It is also shown that the different arc distribution modes observed may impact local solidification times, particularly at the side wall.

DOI: 10.1007/s11663-012-9760-1

I. INTRODUCTION

THE vacuum arc remelting process is extensively utilized in the commercial production of Ti-6Al-4V ingots. Overall, the goal of the process is to increase the homogeneity and purity within the formed ingot. In the first stage of melting, compacted and welded titanium sponge containing the appropriate alloying elements is melted in a VAR furnace in what is commonly referred to as the primary melt. This material is subsequently remelted within a VAR furnace, and if this is the final melt, then it is referred to as a double VAR melt. Some applications, such as rotating parts in jet aircraft engines, require an additional VAR melt, and this is referred to as a triple VAR melt. An intermediate melt stage using an electron-beam (EB) furnace is also sometimes employed.

One advantage of the vacuum arc remelting process over vacuum induction melting, for instance, is better melting rate control. This leads to a more tightly controlled solidification and an overall axially orientated solidification front. Figure 1 shows a cross section of a typical coaxial VAR furnace. The input material, commonly referred to as the electrode, is melted by means of a metal vapor plasma arc that strikes from the electrode to the forming ingot. The furnace is referred to as coaxial when the power supply return feed is attached around the circumference of the crucible flange. Ideally, the effect of this arrangement is that a centered arc will produce no net magnetic field external to the crucible because the current in the crucible is pointed in the opposite axial direction to the current in the electrode. The electrode is the cathode and the ingot is the anode. The primary mechanism for heating *via* arcs is simply concentrated joule heating, and the potential drop across the electrode gap is typically in the 30 V to 50 V range during industrial production. It is important to realize that the arcs do not extensively vaporize the material; rather, the heated material drips off the end of the electrode and into the ingot as a bulk transfer process. For this reason, it is recognized that the VAR process is not as effective at removing some of the heavier type 1 inclusions from the material as compared to EB melting.[1]

The geometry of a VAR furnace is such that there is no direct view of the electrode arc gap region. For titanium alloy melting, gap lengths are on the order of a few centimeters. The positions and in turn distribution of arcs is not directly controlled, and arcs are free to move about. The video cameras looking down the annulus of the furnace give some indication of the arc dynamics. This is monitored by an operator but is typically not used by the automated control system.

The arcs, and more specifically the temporal distribution of arcs, have the potential to impact the forming ingot in several ways. The most obvious way is through the heat flux into the molten pool. There is potential for spatial variations in the overheat if the arcs do not distribute evenly over time. It has been reported that the ideal case is a diffuse arc that evenly distributes a heat flux into the melt pool, and so-called arc constrictions (nonuniform arc distribution) have been linked to the formation of defects in the ingot.[2] However, it should be noted that this was for nickel alloy melting without the presence of a stirring coil. In the VAR of Ti-6Al-4V,

C. RIGEL WOODSIDE, General Engineer, and PAUL E. KING, Business and Outreach Manager, are with the National Energy Technology Laboratory, Albany, OR 97321-2152. Contact e-mail: Rigel.Woodside@netl.doe.gov CHRIS NORDLUND, Quality Assurance and Technology Manager, is with ATI Albany Operations, Albany, OR 97322-3828.

Manuscript submitted January 12, 2011.

Published online: 07 December 2012

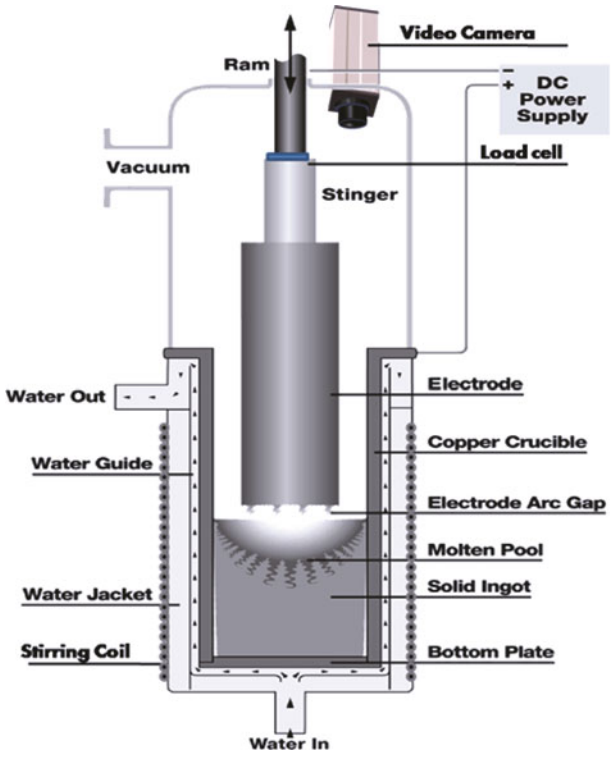

Fig. 1—Cross section of the VAR furnace. Sketch is courtesy of ATI Allvac, with a modification to show instrumentation.

melting rates are much higher than utilized during nickel alloy melting. Thus, the molten pool is quite deep, sometimes being described as having a "soda can" shape. This means the localized heat flux from the arcs will have less impact on the solidification front as compared to nickel melting because of the difference in distances from arc to solidification front. However, arc constrictions toward the side wall can potentially lead to shelf remelting, causing material to fall into the pool, thus the commonly used term "fall-in." This material can remain intact in the melt pool and can be a source for point defects as its composition will often differ from the nominal alloy composition. An example is a type 2 defect characterized as having too much primary alpha phase due to an elevated concentration of aluminum, which is the alpha stabilizer. This leads to a region having slightly elevated hardness as compared to the alloy, and this can be accompanied by a neighboring region having depleted aluminum and lower hardness.

Perhaps a less obvious effect of arc distribution is the effect of the magnetohydrodynamic stirring of the molten metal. In a coaxial furnace design, the electrical current from the arcs enters the melt pool and then largely flows in a radial direction, exiting the ingot near the top of the ingot before moving up the crucible (description in terms of electron flow). The high currents associated with titanium alloy melting create a vigorous convection pattern with a downward flow at the axis of the ingot. This tends to homogenize melt pool temperatures and results in a steep temperature gradient at the solidification front. The convection also mixes the material. The net result can be macrosegregation due to solute partitioning of the alloying elements. Recent results have indicated both through modeling[3] and experimentally[4] that significant Fe macrosegregation occurs during the melting of Ti-10V-2Fe-3Al, and this macrosegregation changes as a function of the total current entering the ingot. The modeling study assumed an axisymmetric and Gaussian distribution of the arc, whether this is valid is one of the aims of the current work.

Perhaps the defect of most concern with Ti-6Al-4V is so called hard-alpha interstitial inclusions, a type 1 low-density inclusion (LDI), because these inclusions can become crack initiation sites leading to premature fatigue failure. The fact that hard-alpha material can have a similar melting point and similar density as compared to the alloy makes it difficult to remove *via* VAR. The term hard-alpha actually refers to material over a range in the Ti-N phase diagram, sometimes referred to as nitrides, and within this range, there is considerable variation in the fracture toughness.[5] Ti-N inclusion "survival" times in a VAR melt pool as a function of particle size and density have been modeled.[6] As mentioned, the arc current drives the fluid motion. An understanding of the fluid dynamics in the pool is critical to predicting the ability of VAR to reduce these defects.[7] Therefore, knowing the VAR arc distribution is in turn critical to making accurate predictions of the dissipation of hard alpha inclusions within the VAR melt pool. Producing ingots free of high-density inclusions (HDI), a type 1 defect consisting of a refractory element such as tungsten, is also important but is expected to be less dependent on arc distribution. This is because these inclusions tend to rapidly sink to the bottom of the melt pool, so changes in the arc driven fluid dynamics are less important.

It is also possible that the arc distribution impacts the physical structure of the ingot sidewall surface. This is significant because the sidewall integrity and grain structure can in turn affect subsequent forging operations and product yield. Multiple techniques are used within industry to improve ingot surface quality, but determining the effect of the arc distribution on the ingot surface has been difficult.

Arc distribution is relevant to the quality of any material melted *via* VAR. The focus on this paper is on Ti-6Al-4V not because this alloy deserves the most attention but rather because of circumstantial convenience in terms of the experiments. The technique described is applicable to other VAR operations, but it should be noted that the reported arc motion and distribution results may be specific to the furnace and procedures followed by ATI Albany Operations (Albany, OR).

A. *The Vacuum Arc*

A vacuum arc is more accurately called a metal vapor plasma arc. The VAR arc is sustained by vaporization and ionization of the electrode material, rather than an ambient gas. In VAR, the two critical components for the arc are the metal vapor plasma and the cathode spot. The cathode spot emanates the bulk of the electrical

current, and its size is extremely small. Spot current densities can vary by orders of magnitude, and it has been empirically observed that an individual titanium cathode spot can only hold up to 70 A before splitting into multiple spots, and even these spots are composed of microspots that may only hold up to 2A.[8] The spots can cluster, appearing from a distance to be a single spot, which might be recognized as the arc. Spots can also repel one another, a phenomenon known as retrograde motion. The term retrograde is used when the relative motion between multiple spots is in the opposite direction of the expected Lorentz force direction arising from the spot's self-generated magnetic field. Another relevant feature is that spot motion is actually not continuous but rather discreet, and a close examination of cathode spots can reveal tiny surface craters. The combined effect of discreet motion, retrograde motion, and a localized fractal nature of spots has been demonstrated in short-term laboratory experiments.[9]

In addition to the current discharge at the spot, there is a diffuse current transfer associated with the plasma. This plasma current, sometimes referred to as the ion current, has been predicted to have a Gaussian distribution about the cathode spot in VAR with a width on the order of a few centimeters.[10] The proportion of cathode spot current to plasma current is not known and estimations vary. The electric current transfer *via* an arc, though, can be thought of as the superposition of transfer by the cluster of spots along with the plasma current transfer. At a distance, the arcs can be thought of as a line source, such that the electrode gap, can be thought of as a circuit that contains resistors in parallel (the arcs). As mentioned, cathode spots move discreetly, but the arc is a collection of spots so the apparent motion can be considered as continuous. The speed of arc movement is important, if the arcs move slowly or are stationary, then magentostatics can be employed, whereas if they move rapidly, then induction effects must be considered. High-speed video evidence in a specially designed furnace showed that spots can move quickly, generally forming in the middle of the furnace and moving with retrograde motion to the edge of the electrode with a time period of about 1 ms.[11] However, the video evidence also showed that arcs can constrict to a side at much slower time scales. Slower arc movement is of greater interest because the effects of rapid arc movements will tend to be attenuated by thermal diffusion speeds of the material as well as the momentum of the flow in the pool.

Mark Ward, who pioneered the use of externally applied magnetic flux density sensors as a means of studying VAR arc behavior, reported observing a slow ensemble arc motion around the axis of the furnace with a time period of 20 to 40 seconds for nickel alloy VAR.[12] This demonstrated that arc distribution can be nonaxisymmetric and non-Gaussian about the center at an instant. It also indicated that a magnetostatic approach can be employed to learn something about arc distribution. Further investigation was performed to assess the relevance of this finding to determine relevant time periods for an arc distribution shift to have an impact on the forming ingot.[13]

Overall, much of what is known about arcs and their behavior is based on empirical observations. Furthermore, the observed behaviors vary considerably, and as remarked by Boxman, it often seems that researchers in the field are studying completely different phenomenon.[8] This makes designing a functional arc position measurement system difficult. Thus, there is a general need to acquire and catalog pertinent external magnetic field information for different VAR operations.

For VAR of titanium alloys, there is some general knowledge of arc distribution and motion in the industry. For instance, it is well known that melt view video seems to indicate that the arc is often rotating, and this rotation direction can switch. This is attributed to the axial magnetic field generated by a DC current "stirring coil" that is wrapped around the furnace. The polarity of the coil is periodically switched, which switches the direction of the axial field inside the furnace. Field strengths, generally less than 10 mT, and switching times vary considerably throughout the industry. Stirring coils are generally not employed in nickel alloy melting, so the VAR arc distribution experiments previously mentioned are not necessarily applicable here.

Further knowledge of distribution comes from observations of melt tips from aborted melts; observations of the stub are not necessarily indicative of the melt as a whole because hot topping is typically performed at lower power. Melt tips are generally not flat; rather, they can be slightly convex, concave, some more complicated profile, or even nonuniform. These differences are likely the result of arc distribution differences, and the aim of the presented methodology is to provide a real-time capable indication of these differences.

II. METHODOLOGY

The basis for determining slowly varying arc locations and in turn arc distribution is the relationship between a current density and a magnetic flux density. The relationship is shown in Eq. [1], known as the Maxwell–Ampere law.

$$\nabla \times \mathbf{B} = \mu \left[\mathbf{J} + \frac{\partial \mathbf{D}}{\partial \mathbf{t}} \right] \qquad [1]$$

In this equation, $\mathbf{B}$ is the magnetic flux density vector, μ is the magnetic permeability of the medium through which the field is propagating, $\mathbf{J}$ is the current density vector, and $\partial\mathbf{D}/\partial t$ is the rate of change of the electric field vector, which is sometimes referred to as the displacement current. The furnace power supply provides well rectified direct current (DC). In general, electrical processes varying at a rate up to 60 Hz can be described using magentostatics formulations without introducing much error.[14] So the displacement current $\partial\mathbf{D}/\partial t$ is neglected (assumed to be zero). The complexity in using the Maxwell–Ampere law to find an arc, though, arises because the movement of the arc also causes the current paths in the rest of the furnace to

change. Thus, the magnetic flux density external to a furnace is a function of these sources in addition to the flux generated by an arc.

A. *Finite-Element Modeling*

To describe the complex relationship of the current paths, COMSOL Multiphysics (COMSOL, Burlington, MA), a general finite-element analysis (FEA) software package, was utilized. COMSOL solves problems using the finite element method with partial differential equations.[15]

Thermal or magneto-hydro-dynamic processes were not modeled in the FEA. These processes are important to VAR operation but can be neglected in the model because they have a negligible effect on the external magnetic flux density as compared to that arising from the changing current paths due to arc movement.

A three-dimensional (3-D) model of the furnace and the experimental setup, including sensor locations, was created. Multiple states are needed to account for varying ingot heights and varying arc locations. The entire model geometry is meshed with greatest detail in the arc region to create the discrete finite elements.

In solving the problem, a finite-element electrostatic equation is first utilized to determine the current density throughout the geometry resulting from an arc position. The electrical conductivity in the electrode gap outside of the arc was set to a value near zero, which forces all of the current through the arc in the model. The ingot was modeled as an ideal cylinder; no assumptions were made as to the boundary resistance between ingot and crucible. Still, the current almost entirely exits the ingot near the top of the ingot because this is the shortest path, a result that is consistent with current paths experimentally determined by means of placing electrodes on the crucible during industrial titanium VAR melting.[16]

The electrostatic solution is then input into the magnetostatic finite element equation which solves for the magnetic flux density. The output of each model is the magnetic flux density at each sensor location as a function of various arc location scenarios. Figure 2 shows an overhead view of a model, as well as the normalized sensor response as a function of arc position for a single arc.

There are several aspects of the system that simplify approaches of directly solving for arc positions. The materials of construction of the furnace utilized all have relative permeability near one, so the magnetic field arrives at the sensor undistorted. Also, the magnetic field linearly scales with increasing current for a given arc position. Finally, principles of superposition can be utilized so that the effect of multiple arcs can be predicted by simply superimposing the results for individual arcs at the same locations. Superposition and linearity of the current have been taken advantage in a recent paper by Ward *et al.* that determined arc positions from a discrete map of FEA results as a function of arc positions.[17] An algorithm was employed that solved the forward problem to find the best solution for arc positions.

In this article, we build on an approach of using a continuous arc position solution that is based on fitting the FEA results into furnace specific forms of the Biot-Savart law.[18] Continuous arc position equations are desirable so the results are not limited to arc positions simulated in the FEA. This also makes excessive finite-element simulations unnecessary. Finally, the arc position determination method presented below has some advantages when working the inverse problem; for instance, there is an exact deterministic solution for a single arc position from a single *x-y* magnetic flux density sensor.

B. *Arc Position Determination*

In a magnetostatic derivation of the Maxwell–Ampere law, the relation between superimposed line sources of current (the arcs), and a magnetic flux density vector at a point (the sensor) is described by the Biot–Savart law as shown in Eq. [2].

$$\mathbf{B}(\mathbf{r}) = \frac{\mu_0}{4\pi} I \int \frac{d\mathbf{l}' \times \hat{\eta}}{2} \qquad [2]$$

$\boldsymbol{B}$ (Teslas) is the magnetic flux density vector at a point r, the integration is along the current line in the direction of flow, $d\boldsymbol{l}'$ is an element of length (m) along the total current I (Amps), and $\boldsymbol{\eta}$ is the vector from the source to the point. μ_0 is the permeability of vacuum. Further simplification can be made if the line sources are straight and pointed in a known direction. For VAR arcs, the gap length is short, on the order of a few centimeters, *vs* the diameter of the electrode, which is on the order of a meter. So it is difficult to fathom arc discharges taking a path that would significantly vary from being collinear with the axis of the furnace. The exception being side-arcing, but this is avoided.

This aspect, along with the axisymmetry in the furnace's geometry, yield the Biot-Savart based Eqs. [3] and [4] in a polar coordinate system.

$$B_t = m_t I\left(\sum_{i=1}^{n} \frac{f_i \sin\theta_i}{d_i} - \frac{1}{r_s}\right) \qquad [3]$$

$$B_r = m_r I\left(\sum_{i=1}^{n} \frac{-f_i \cos\theta_i}{d_i}\right) \qquad [4]$$

B_t and B_r are the magnetic flux densities (T) at a sensor in an orientation as indicated in Figure 3. θ is the angle from the sensor to the arc, d is the distance from the sensor to the arc (m), r_s is the distance from the sensor to the center of the furnace (m), I is the total circuit current (Amps), f is the fraction of the total current associated with the arc, and n is the number of arcs present. The terms m_t, m_r are referred to as furnace response coefficients and have units that are the same as that for magnetic permeability (N/A^2). They are determined by a regression fit of FEA generated data into the equations. Essentially, these terms account for the fixed length of an arc and approximate the magnetic effect of

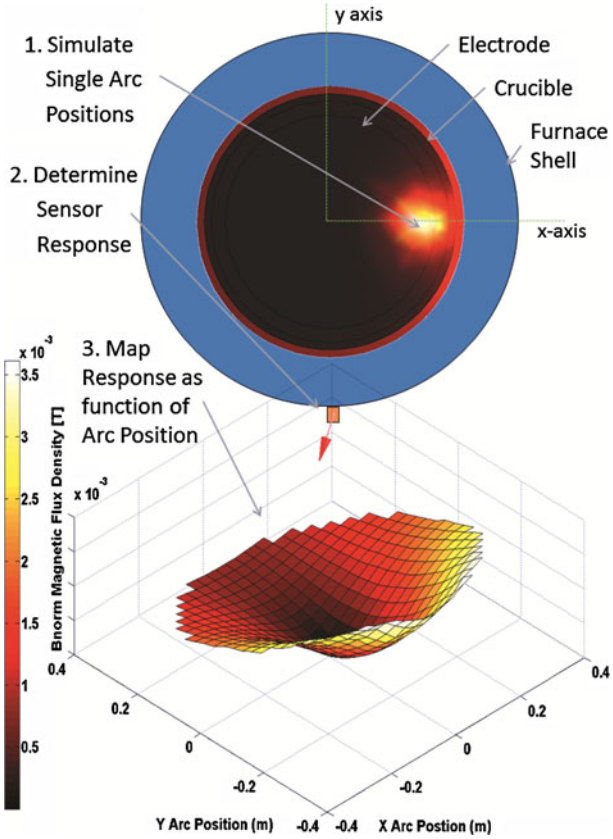

Fig. 2—At the top is an overhead view of the current density just below the ingot surface as determined by the FEA for a single-arc simulation. At the bottom is the magnitude of the normalized magnetic flux density vector for a sensor located at an *x*-*y* coordinate of (0, –0.64) as a function of the position of a 35-kA arc center.

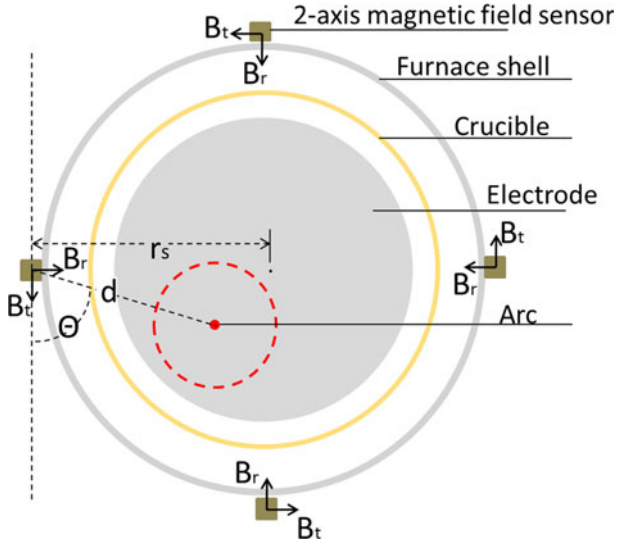

Fig. 3—Diagram of the setup for arc position determination. Determination is insensitive to the arc diameter, as indicated by the dotted line.

Table I. Furnace Response Coefficients and Radial Sensor Location Utilized

m_r (N/A^2)	m_t (N/A^2)	r_s (m)
9.0×10^{-8}	4.9×10^{-8}	0.64

the arc position dependent current paths through the rest of the furnace geometry. In an ideal coaxial furnace, a centered arc produces zero net magnetic field outside of the furnace, thus the $1/r_s$ term. Each sensor has an Eq. [3] and [4], and for an array of sensors about a circle m_t, m_r, f_i, r_s, n and I will be the same for each. Figure 3 shows the setup. In the convention used, B_r is pointed toward the center, such that θ is always between 0 and 180 deg. I, total system current, is positive and pointed out of the page.

It is important to realize these formulations are for the electrode side of the gap. To maintain conservation of charge, it is known that the measured total system current travels through the electrode. But it does not necessarily travel through the ingot. This is because some of the current is transferred directly to the crucible *via* the metal vapor plasma associated with an arc. The current transfer in the plasma is more diffuse than the discharge from the cathode spot, even though the plasma is generated by the spot. Correct accounting for the plasma is certainly relevant to arc position determination, given that it has been shown that the direct electrode to crucible current transfer could be on the order of 30 pct of the total current during industrial titanium VAR.[16] Most of the current appeared to be entering the crucible near the top of the ingot, so there was a fairly large uncertainty in this determination. It is not unreasonable to assume that much of this current came off the end of the electrode rather than the side because the plasma is generated by the spots and because side-arcing is avoided. The B_z field is the most sensitive to spatial variations in the radial current, which is a reason not to use it in the arc position determination. As predicted by the FEA, the B_r and B_t tend to be flat as a function of axial distance from the arc plane when this plane is coincident with the sensor plane, whereas the B_z is linearly changing. Therefore, the m_r and m_t terms can be considered as constant over an ingot length change when the sensors are close to the arc without introducing much error. The values used in this study can be seen in Table I, utilized over an ingot length change of about 15 cm.

The formulated equations are essentially furnace-specific forms of the Biot–Savart law that relate electric line sources to the magnetic field vector at a point. For these experiments, it was expected that the number of arcs present exceeded the number of sensors (4); thus, the problem is underdetermined. Still, it will be shown that a single-arc method can be an effective means of detecting arc-distribution differences.

C. *The Single-Arc Method*

The single-arc version of Eqs. [3] and [4] can be inverted to give an exact arc position from a single sensor using Eqs. [5] and [6].

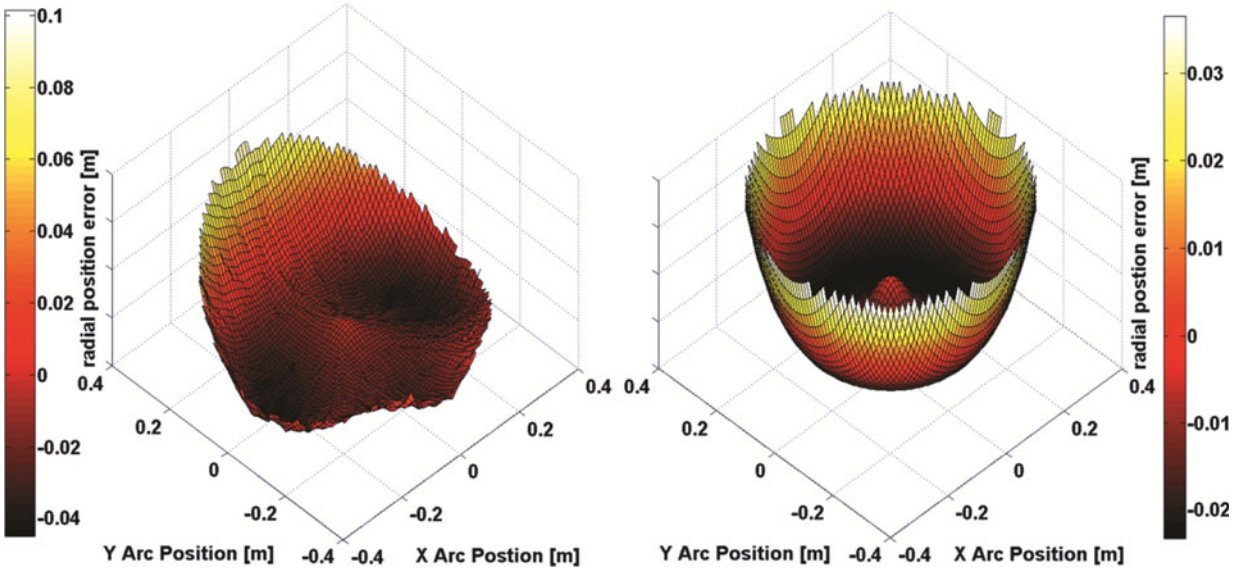

Fig. 4—The radial position difference (error) between FEM arc locations and calculated arc locations using the single arc method. At the left is the error for a single sensor located at (0, –0.64). At the right is the error when averaging the position data from the four sensors.

$$d = \frac{I m_r m_t}{\sqrt{\frac{I^2 m_r^2 m_t^2}{r_s^2} + \frac{2IB_t m_t m_r^2}{r_s} + B_r^2 m_t^2 + B_t^2 m_r^2}} \quad [5]$$

$$\theta = \cos^{-1}\left(\frac{-B_r d}{m_r I}\right) \quad [6]$$

The terms are the same as previously discussed and as shown in Figure 3. To improve the accuracy of arc location determination, the found arc position using Eqs. [5] and [6] for each sensor are averaged to give a final position result.

The equations are imperfect approximations, but the error between the more accurate FEA and the equations can be quantified. For the single-arc method, the difference between the simulated single-arc radial positions in the FEA and the found arc radial positions using the equations can be seen in Figure 4.

Essentially, this is a plot of residuals for the fit of FEA generated data into Eqs. [3] and [4]. This demonstrates how the problem can be simplified while introducing minimum error to quickly arrive at a solution using Eqs. [5] and [6]. There is negligible (less than 5 mm for a single sensor and less than 1 mm for the average of 4 sensors) position error in the azimuthal direction. Since the radial and azimuthal errors are systematic and known, they can be corrected for if increased accuracy is desired. It should be noted that this does not give an indication of overall arc position accuracy. The accuracy in arc position determination will be dependent on a multitude of factors, and as will be later discussed, the largest uncertainty arises because the number of arcs present in the system at an instant is unknown.

Although a single point is located, an identical result will be found if there are multiple arcs with local axisymmetry about the predicted point. Thus, when faced with multiple arcs, the single-arc method yields position data for something that might be called the center of the arcs. This center represents the center of the total current flux. Essentially, the center of the arcs as determined by the single-arc method is the centroid of the current being conveyed by the arcs.

D. *The Experiments*

Eight 3-axis Hall Effect sensors having a measuring range of ± 50 mT and a bandwidth of 20 kHz were utilized. The axes are orthogonally oriented and closely spaced so that a magnetic flux density vector can be determined for each sensor. The sensors were placed on the outside of a commercial VAR furnace at the ATI Albany Operations in two planes of four sensors each. During a melt, the electrode gap moves up the axis of the furnace as the ingot length grows, so there ends up being two times during a melt where the gap was coincident with a plane containing four sensors. The sensors were arranged symmetrically about the circumference.

In addition to the magnetic measurements, the furnace voltage, current, and stirring coil current were acquired. This data were sampled and recorded at either 3.0 kHz or 3.7 kHz. Two rates were used to ensure any consistent periodic behavior observed was not the effect of digital aliasing. The data presented were processed with a 25 Hz low pass filter and resampled to 50 Hz.

The data presented are for final Ti-6Al-4V heats (melts). The exact operation parameters of each heat are propriety, but it can be said that current was greater than 30 kA, voltage 30 to 50 V, and stirring coil operation low with moderate reversal times. The magnetic field at a sensor due to the stirring coil current was negated from the measurements by running the coil prior to striking an arc and determining an offset as a function of coil current.

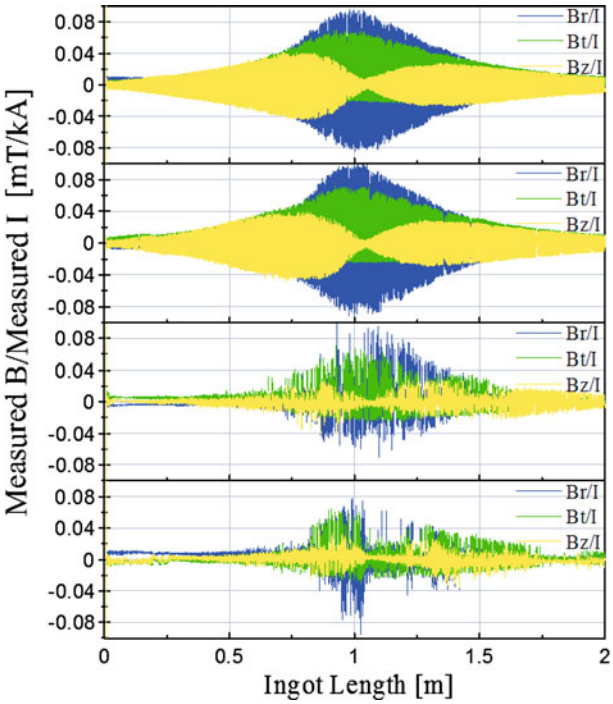

Fig. 5—Waveforms of experimental results showing the signal due to arc movement during four final Ti-6Al-4V VAR heats. The magnetic sensor was located at a position corresponding to an ingot length of about 1 m. The VAR process parameters were the same for each.

ATI Albany Operations provided internally acquired electrode weight data, ram position data, vacuum pressure, and melt view video. The electrode ram position data and the electrode weight data, along with the electrode's density and system dimensions, were used to calculate the ingot length during the melt.

III. RESULTS AND DISCUSSION

The experimental results from final production VAR heats of Ti-6Al-4V are presented. The final melts are of particular interest because they represent the last solidification step for the material. The furnace VAR operation parameters (*e.g.*, target melt rate, voltage, stirring coil current, *etc.*) and sensor positions were the same for each. Still, there were some differences in the processing route from raw material to final melt. There were also slight differences in the electrode diameters and final ingot lengths, but the crucible lengths and ingot diameters are the same for each heat presented.

A. *Arc Magnetic Signature*

It is expected that the measured magnetic field will be zero for either the case of a single arc centered in the exact middle of the furnace or for a diffuse collection of arcs with axisymmetry about the middle of the furnace. This should be the case regardless of the value of the total current. This aspect is particular to furnaces of coaxial design. If the arcs move to one side of the furnace, then a nonzero field is created external to the furnace, and this field is expected to linearly scale with the total system current. The signal of interest is the magnetic field that changes due to the movement of the arcs, as opposed to the magnetic field changes due to current fluctuations. Therefore, we can visualize the signal of interest, arc movement, by dividing the measured magnetic flux density by the measured total system current. The results plotted as a function of the ingot length are seen in Figure 5. Generally, the change in ingot length is fairly linear with the change in time for the data shown.

Overall, it can be seen that the shape of the waveforms differ. The waveform at the top of Figure 5 shows the greatest arc movement, and the shape is similar to that predicted by the finite element model (FEM). The highest signal-to-noise ratio can be found when the electrode gap is in line with the sensors, for this sensor it is at an ingot length of approximately 1 m. As the electrode gap moves away from the stationary sensors, the signal decreases and part of the magnetic field emanating from the arcs moves to the z-axis. B_z was measured, but it is not utilized in this article. It is readily evident in the magnetic signature that there are differences in the arc behavior among the different heats. This is important because it demonstrates that monitoring the external magnetic fields during VAR has the potential of providing new insight into variations of the process.

B. *On the Number of Arcs*

Perhaps the most significant challenge to the measurement system is that the number of arcs present at an instant is unknown. Although unknown, we can learn something about the number of arcs from the data. Consider the case where the arcs are centered about the middle axis of the furnace. If there were a single arc or if there were hundreds of arcs, then the result would tend to be the same: All sensor elements would read zero field and the single-arc calculations from the different sensors would agree that the arc location was in the exact middle of the furnace. Such an arrangement of a multitude of arcs is the expected outcome of the central limit theorem. Indeed, this forms the basis for the traditional idea of a Gaussian arc distribution.

Systematic errors, for instance those associated with the current measurement, tend to be negligible when the arcs are centered. Thus, it is advantageous to exam data consistent with centered arcs. Centered arc sensor agreement can be seen in the data. However, what is far more prevalent is disagreement in arc position among sensors on the order of 0.05 m to 0.1 m, and these distances change during short time scales.

Centered arc agreement would also be the case if there were a large number of arcs in a ring. Retrograde motion may then be difficult to measure. However, if the number of arcs were few, then the arc position predictions from the different sensors would move with retrograde motion. This phenomenon was observed in an earlier study with a laboratory scale furnace, although in that case, much higher frequency behavior was also observed.[18] For these experiments, retrograde motion is not observed, and the data generally show

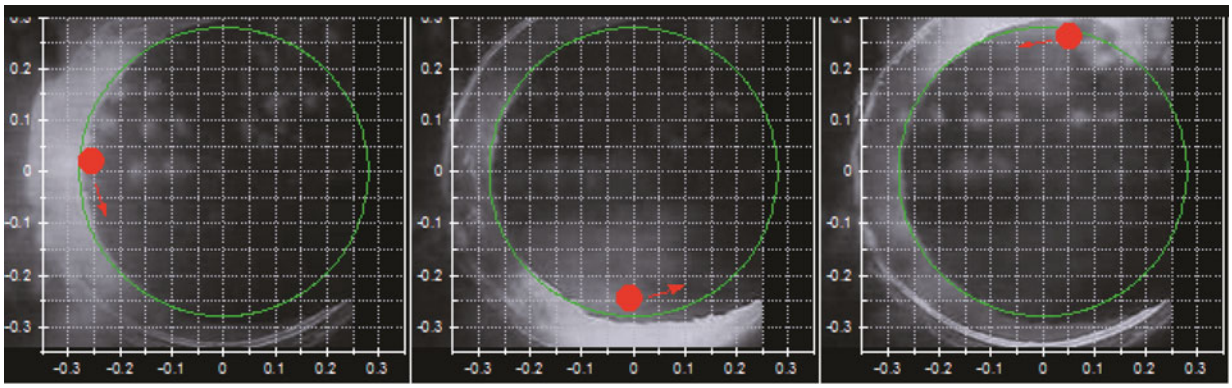

Fig. 6—Determined arc position superimposed on top of three video frames spanning a period of less than 20 s. The arrow indicates the direction of arc motion as observed in both the video and the arc postion data.

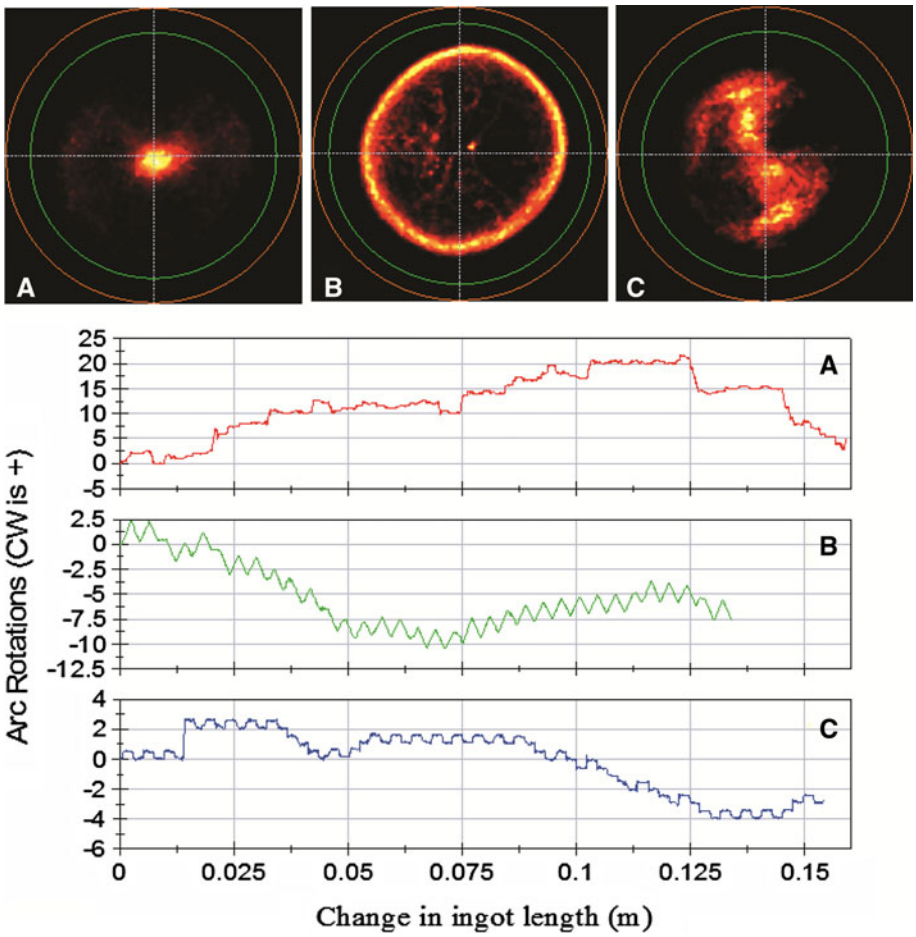

Fig. 7—Three types of arc distribution and motion observed during final Ti-6Al-4V VAR. Distribution is shown by color intensity (hot color map) corresponding to the number of insistences the arc center was found at the corresponding position. The inner circle represents the electrode and the outer circle the crucible. Azimuthal arc motion is shown in terms of arc rotations where one rotation is 2π radians. The view is looking down the axis of the furnace.

sympathetic motion among the sensors. Yet over intermediate time scales, the positions of the arcs from different sensors can move relative to one another. The only known explanation for this is the presence of multiple arcs. The movement is much greater than noise; the effect of noise is at a scale of around 1 mm of displacement. This is consistent with a finite number of arcs greater than one that are detectable with the described arc position determination methodology.

Equations [3] and [4] can be solved for as a forward problem by finding solutions with a minimum root sum of squares (RSS) between the measurements and the

calculations. If it is assumed that each arc carries equal current, then the number of unknowns is equal to the number of sensors if it is also assumed that the number of arcs is equal to the number of sensors. This provides a framework for solving the problem when there is a much greater number of sensing points than arcs because a solution for 32 equal arcs will be the same as a solution for 16 equal arcs if the correct answer is 16 equal arcs for instance. Given that current amounts in arcs are thought to be multiples of a material dependent discreet amount, this makes some physical sense. Of course, there still is a practical amount of arcs that can be detected, and this is determined by the measurement accuracy and resolution.

For these experiments, there were only four sensors. The forward problem was solved for and solutions were found that had lower RSS than the single-arc solution. Two arcs, carrying equal current, do yield a significantly lower overall RSS.[19] However, it cannot be proven with the information available that the multiple arc solutions represent accurate arc positions. Whether there is some constant diffuse current associated with the plasma that is magnetically silent also cannot be determined. This is of interest, and an expected outcome from this effect on a solver utilizing a large number of sensing points would be an excess of arcs found in the center. In terms of a diagnostic of arc motion and distribution, though, the single-arc method seems to be effective.

C. *Arc Position Validation*

The arc position determinations using the single-arc method were compared to melt view video. The camera looks down the axis of the furnace, as shown in Figure 1, and can see an annulus of the melt pool surface that is in view between the electrode and crucible. Gross movement of arcs can be observed, such as when they gather together on one side of the electrode. A sequence of three video frames from a primary melt, with a determined arc position superimposed can be seen in Figure 6. A primary melt was selected because the large crucible to electrode diameter ratio yields a better view than experienced during final melting. This gives some confidence that the methodology is being correctly implemented and the system is capable of tracking gross arc movement.

D. *Arc Motion and Distribution*

Using the single-arc method, *x*-*y* arc position data were converted into polar coordinates. These data points were examined to determine which quadrant they were located in so that arc motion angle data are accumulative rather than simply having a value between 0 and 2π. Consecutive data points from quadrant 1 to quadrant 3, for example, are ambiguous in their rotation direction so they were treated as alternating rotation values of π or $-\pi$ so as to minimize any accumulated error associated with this ambiguity. Fortunately, very few consecutive data points required this treatment. To visualize a time averaged distribution, *x*-*y* arc position data were processed with a two-dimensional (2-D) histogram having a bin size of 1 cm × 1 cm. The bin size is somewhat arbitrary and simply chosen to highlight arc-distribution differences. Figure 7 shows three different arc rotational motion and arc-distribution patterns observed during final Ti-6Al-4V VAR over an ingot length change of about 15 cm.

The pattern for A is consistent with that which would arise from a diffuse collection of arcs providing a centered distribution of energy into the ingot, as has traditionally been used in solidification models of the VAR process. Interestingly, there appears to be a net rotation about the center of the furnace in one direction or another, and this rotation does not appear to be affected by the stirring coil. When examined over shorter time scales, it is also apparent that the distribution is often not axisymmetric at an instant and the characteristic distribution pattern takes some time to develop.[20] The time period for a single rotation about the center of the axis is primarily in the 1- to 20-second range. Radial motions of arcs over the same time scales were also observed. Pattern B indicates that a greater amount of current is entering the ingot near the side wall (with the crucible) as compared to pattern A. Additionally, the arc rotates with a fairly consistent speed about the axis of the furnace as indicated by the triangular shape in the arc rotation plot. The direction switch directly corresponds to the switching of the stirring coil polarity, which indicates that the axial field generated by the coil is driving the motion direction. A net motion about the center is also observed with this pattern. Pattern C was only predominantly observed during one of the final melts examined. For pattern C, the arc makes half a rotation about the center axis with each stirring coil polarity switch, and appears to stick at two positions 180 deg apart from one another. This rocking back and forth leads to the square wave looking rotation plot and the "wing" distribution pattern. In terms of the magnetic signature, as shown in Figure 5, a melt dominated by the "center" pattern A or the wing pattern C appears like the bottom two plots, whereas a melt dominated by the ring pattern B appears like the top two plots. Overall, it is apparent that a particular heat seems to prefer a particular pattern or arc-distribution mode. It is interesting to discover this, considering the same alloy is being melted in the same furnace with the same VAR operation parameters. It is believed, therefore, a heat's preferred arc-distribution mode has more to do with differences in the processing of the electrode pre-VAR, rather than differences in the VAR process operation parameters.

E. *Arc Position and VAR Operation Parameters*

Even though there are overall differences in the arc motion and distribution amongst heats, this is not apparent in the system current, voltage, or stirring coil. In other words, those parameters are not good indicators of which distribution mode is dominant. This indicates that the measurement system is providing new information. Changes in arc distribution and motion are also observed during a melt. For example, what appears to be signal drop outs in the top two magnetic signatures

shown in Figure 5 are actually changes from a ring mode to a center arc-distribution mode. Even though there is no overall correlation between arc position and system voltage, a trend in this correlation is apparent for individual heats. Generally, VAR system voltage corresponds to the electrode gap length with a larger voltage representing a larger gap length. Figure 8 shows a color map plot for voltage *vs* determined *x-y* arc positions for two different heats.

It is conceivable that the differences seen in Figure 8 correspond to an effect of an uneven electrode. So the top plot has the highest voltage in the center because the arcs are concentrated in the center causing the electrode to be slightly concave, whereas the plot shown in the bottom has the highest voltage near the edges because the arcs are concentrating there. So in this case, the electrode tip might have more of a convex shape.

F. *Arc Distribution Effect on Solidification*

In the VAR of Ti-6Al-4V, the largest impact of the arc distribution in terms of the solidification is expected to arise from the changes in the magnetohydrodynamic stirring due to changes in the arc distribution. BAR, a 2+D axisymmetric solidification code developed by researchers at the Sandia National Laboratory, was utilized. Experimental validation of BAR has shown that it can effectively model the VAR of Ti-6Al-4V, as is the case with the current work.[21] Although a full description of the effect of VAR arc distribution would require a 3-D model, the 2+D can at least give indication whether the observed arc-distribution differences are capable of yielding solidification differences. The + is in the description because the code considers physics acting in 3-D, but the mesh and boundary conditions are 2-D axisymmetric. The BAR code allows for 2-D axisymmetric piecewise input for the current flux into the ingot, and this was utilized.

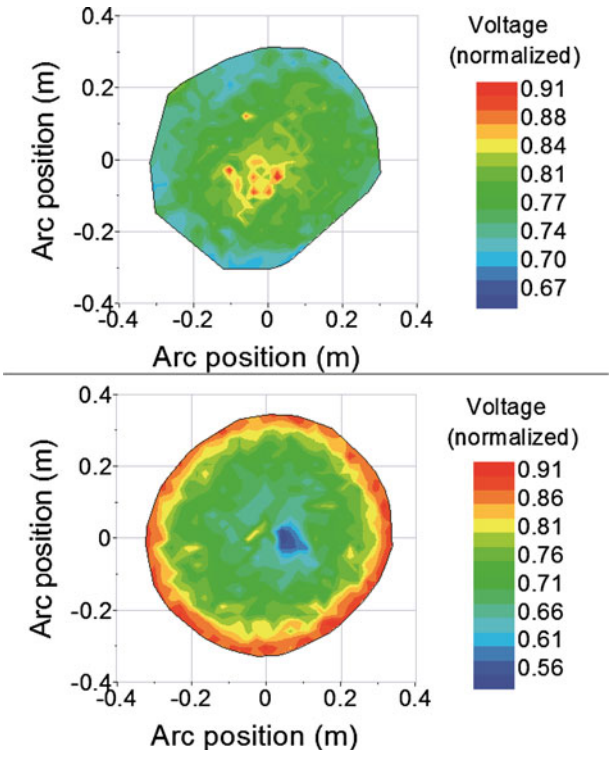

Fig. 8—Relation of furnace voltage to arc position. At top is the relation typically seen for heats dominated by a centered arc distribution, and at bottom is a correlation typical for heats dominated by a ring distribution.

To arrive at the axial current density entering the ingot from the measured data, some assumptions are needed. The described method essentially locates points, so an arc diameter must be assumed. The arc-distribution patterns observed generally show clearly defined circular patterns and the electrode is also circular. This gives evidence that the arcs may have a consistent extent. For the ring distribution mode, the arc position results were usually about 10 cm from the edge. So it is assumed that the extent of the arcs is over a diameter of 20 cm. The extent of arc position predictions for the center distribution mode was within about 10 cm from the edge, so the arc was again assumed to have a diameter of 20 cm. From the single-arc method, arc radial position is averaged and processed with a one-dimensional (1-D) histogram. These data were then divided by the corresponding circumference at the radial position to arrive at a distribution of arcs per area as a function of radius. A moving average was then used to smooth the data across the radius. This ends up being the equivalent of considering the arc as providing a square distribution of current density over a circle having a 20-cm diameter. The final result is a time averaged, 1-D axisymmetric, current density at the electrode tip.

It is fairly established that some of the current exiting the electrode travels directly to the crucible *via* the metal vapor plasma rather than entering the ingot. Estimates for the amount of this current vary. Electrodes placed on the outside of a VAR crucible during noncoaxial Ti-6Al-4V VAR suggested this current was about 30 pct of the total,[16] whereas a numerical study estimated this current was about 20 pct of the total.[22] The impact of this phenomenon on the determined electrode tip current density profile is expected to be a slight bias of the data toward the center of the furnace. It is slight because the method is not particularly very sensitive to variations in the location of the radial current density. So in the solidification model, the relative current density profile entering the ingot top can be assumed to be the same as the determined relative current density profile at the electrode tip. The total current entering the ingot top was assumed to be 75 pct of the measured total VAR current.

In order to learn specifically about the effect of current distribution, it was assumed that the heat flux and mass flux was independent of the current flux. Both the heat flux and mass flux were assumed to be uniform across the top of the ingot. Assuming this for the heat flux is not a good assumption, but the localized heat flux is not expected to have a large impact at the solidification front because of the pool depths involved when melting Ti-6Al-4V. The results for two simulations are presented: first, for the estimated current density into the

Table II. Selected Solidification Model Parameters Utilized

BAR Solidification Model Parameter	Value
Percent total current entering top of ingot	75 pct
Percent total power entering top of ingot	50 pct
Temperature of liquid metal entering top of ingot	2100 K (1827 °C)
Temperature of alloy liquidus line	1933 K (1660 °C)

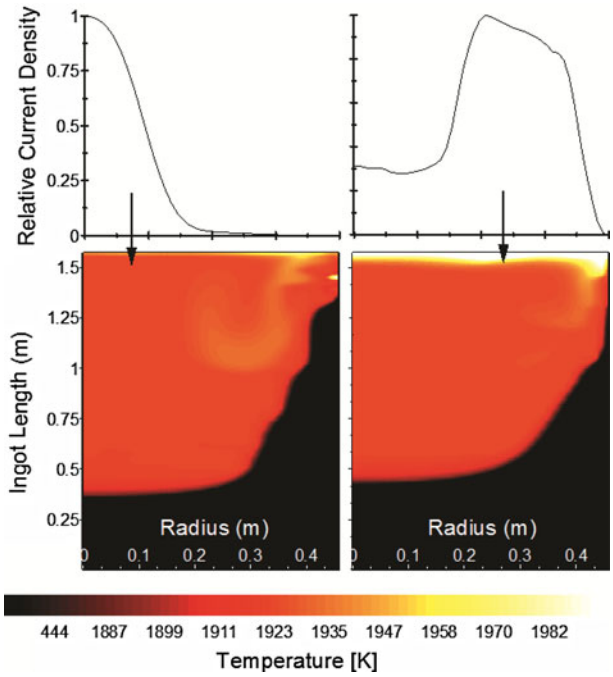

Fig. 9—The temperature profile in the liquid and mushy zones for two cases of VAR melting of Ti-6-4. The case on the left is for the predicted current density into the ingot for the center arc-distribution mode, and the case on the right is for the ring distribution mode. The distribution was considered axisymmetric and constant over the duration of the melt.

ingot from the center distribution mode observed and second for the estimated current density into the ingot for the ring distribution mode. The furnace current, melting rate, and power efficiency were assumed to be constant and the same for both cases. Thus, the only difference between the two models is the current density distribution into the ingot. There was also an assumption that the distribution was constant over time. Thus, the data generated are somewhat fictionalized and simply intended to highlight potential differences. Table II lists some relevant parameters for the solidification model.

The assumed power efficiency and overheat of the metal entering the top of the ingot is the same as used in another relevant solidification modeling effort.[22] The efficiency value is also in good agreement with an experimentally determined average value. The specific heat and latent heat of fusion are known thermophysical properties of the alloy, so the associated energy requirements to heat and melt can be compared to the measurements of furnace power and melt rate. The ingot shrinks and pulls away from the crucible as it solidifies. The liquidus line for the alloy is at 1933 K (1660 °C); for temperatures above that, it was assumed that the thermal and electrical contact resistance was good and constant. The contact resistance was gradually increased for temperatures below 1933 K (1660 °C).

The model can output a variety of useful parameters such as temperature profiles at an instance during the melt. Figure 9 shows the temperature profile of the liquid and mushy zones for an ingot length of approximately 1.6 m. In Figure 9, the color black is solidified material. It can be seen that the pool temperatures are fairly uniform; this is due to the vigorous magnetohydrodynamic stirring. Overall, the main difference can be seen in the shape of the pool near the sidewall. This results in significant differences in the local solidification times. So it is predicted that the side wall "chill zone" covers a larger area for heats dominated by the center distribution mode as compared to heats dominated by the ring distribution mode. Consequently, it is expected that the sidewall integrity and grain structure may be influenced by the arc-distribution mode. It then follows that the arc distribution can have relevance to the subsequent forging process and product yield. Flow related macrosegregation may also be different, but this was not examined in this study.

IV. CONCLUSIONS

This article describes the arc distributions observed during the industrial VAR production of Ti-6Al-4V. Arc distribution and motion were determined by a noninvasive measurement system based on externally mounted magnetic flux density sensors. Refinement of the measurement system to locate all the arcs present remains a work in progress. Still, some new insight into VAR arc behavior is reported. The following conclusions can be made.

There is significant arc position information in external magnetic field measurements at frequencies below 25 Hz during industrial VAR titanium alloy production employing a stirring coil. The data were consistent with the presence of multiple arcs at an instant. The application of four sensors could not conclusively locate all the arcs present, which is not surprising, but the results were consistent with a finite number of arcs that could be located if additional sensors were applied.

The described single-arc method was used to identify three different arc-distribution patterns during final Ti-6Al-4V melting. It is proposed that the observed patterns represent different types of arc-distribution modes. There is the center distribution mode in which the arcs are concentrated in the middle of the furnace. For this case, the stirring coil does not have an obvious effect on arc motion. There is the ring distribution mode in which the arcs are concentrated toward an edge and exhibit a constant speed rotation about the center axis that appears to be driven by the stirring coil. Last, there is the wing distribution mode that appears to be affected

by the stirring coil but only through half rotations, or a rocking back and forth motion. For all three modes, the time periods for rotational motion are generally in the 1- to 20-second range per rotation. A net arc rotation about the center was observed for all three modes; the cause or significance of this is not known at this time.

Individual melts can show correlation between voltage and arc position, which may relate to the shape of the electrode tip as it is being consumed. However, there does not appear to be any overall correlation between VAR operation parameters and the prevalent arc-distribution mode present. This indicates that the measurement system is providing new information. With feedback from the measurement system, the gap length or stirring coil current could be modified in order to achieve the desired arc distribution. Identification and avoidance of defect favoring arc-distribution modes during melting could lead to lower incidences of rejected ingots and improved quality control. The single-arc method utilized is simple, cost effective, and can be retrofitted on existing furnaces. It is already capable of real-time monitoring.

The potential effect of two of the observed arc distributions on the solidification was examined using a 2 + D axisymmetric solidification code. The vigorous convection patterns associated with the arc current predicts minimal temperature variations within the molten pool for either case. However, the different distribution modes do appear to result in different melt pool shapes. This leads to differences in local solidification times, particularly at the side wall. Therefore, arc-distribution monitoring may also provide use toward achieving better side wall quality in Ti-6Al-4V VAR ingots.

ACKNOWLEDGMENTS

A portion of this work was supported through a cooperated research and development agreement between the Specialty Metals Processing Consortium and the United States Department of Energy's National Energy Technology Laboratory. The authors acknowledge the help from the personnel at ATI Albany Operations. Thanks to Steve Henrickson for assistance in interfacing with the existing instrumentation, and Mike Whaley for providing and reducing internally acquired data.

REFERENCES

1. C.E. Shamblen: *Industrial Heating*, 2002, vol. 69, pp. 49–52.
2. F. Zanner, R. Williamson, and R. Erdmann: *International Symposium on Liquid Metal Processing and Casting*, Santa Fe, NM, 2005, p. 13.
3. D. Zagrebelnyy and M.J.M. Krane: *Metall. Mater. Trans. B*, 2009, vol. 40B, pp. 281–88.
4. Z. Yang, H. Kou, J. Li, R. Hu, H. Chang, and L. Zhou: *J. Mater. Eng. Perform.*, 2010, vol. 20, pp. 65–70.
5. K.S. Chan, L. Perocchi, and G.R. Leverant: *Metall. Mater. Trans. A*, 2000, vol. 31A, pp. 3029–40.
6. J.A. Van Den Avyle, J.A. Brooks, and A.C. Powell: *JOM*, 1998, vol. 50, p. 22.
7. G. Ghazal, A. Jardy, P. Chapelle, and Y. Millet: *International Symposium on Liquid Metal Processing and Casting*, Santa Fe, NM, 2009.
8. R.L. Boxman, D.M. Sanders, and P.J. Martin: *Handbook of Vacuum Arc Science and Technology: Fundamentals and Applications*, Noyes Publications, Park Ridge, NJ, 1995.
9. A. Anders: *IEEE Trans. Plasma Sci.*, 2005, pp. 1456–64.
10. P. Chapelle, H.E. Mir, J.P. Bellot, A. Jardy, D. Ablitzer, and D. Lasalmonie: *J. Mater. Sci.*, 2004, vol. 39, pp. 7145–52.
11. F. Zanner, L. Bertram, C. Adasczik, and T. O'Brien: *Metall. Trans. B*, 1984, vol. 15B, pp. 117–25.
12. R.M. Ward, B. Daniel, and R. Siddall: *International Symposium on Liquid Metal Processing and Casting*, 2005, p. 49.
13. D.M. Shevchenko and R.M. Ward: *Metall. Mater. Trans. B*, 2009, vol. 40B, pp. 263–70.
14. D. Griffiths and R. College: *Introduction to Electrodynamics*, Prentice Hall, Englewood Cliffs, NJ, 1999.
15. Comsol Multiphysics 3.1 Users Guide, 2005.
16. R.L. Williamson, G.J. Shelmidine, and J.P. Maroone: *International Symposium on Liquid Metal Processing and Casting*, Santa Fe, NM, 2005, p. 29.
17. B.G. Nair and R.M. Ward: *Meas. Sci. Tech.*, 2009, vol. 20, p. 129901.
18. R. Woodside: Masters Thesis, Oregon State University, Corvallis, OR, 2008.
19. R. Woodside and P.E. King: *International Instrumentation and Measurement Technology Conference*, 2010.
20. R. Woodside and P. King: *International Symposium on Liquid Metal Processing and Casting*, Santa Fe, NM, 2009.
21. R.S. Minisandram, M.J. Arnold, and R.L. Williamson: *International Symposium on Liquid Metal Processing and Casting*, 2005.
22. J.P. Bellot, P. Zabeti, H.E. Mir, J. Jourdan, P. Chapelle, and A. Jardy: *International Symposium on Liquid Metal Processing and Casting*, Santa Fe, NM, 2009.